Global Health & Medicine. 2023; 5(5):278-284.
ORIGINAL ARTICLE
DOI: 10.35772/ghm.2023.01050

Assessment of skeletal muscle using deep learning on low-dose CT images

Yumi Matsushita[1,*], Tetsuji Yokoyama[2], Tomoyuki Noguchi[3], Toru Nakagawa[4]

[1] Department of Clinical Research, National Center for Global Health and Medicine, Tokyo, Japan;
[2] Department of Health Promotion, National Institute of Public Health, Saitama, Japan;
[3] Department of Radiology, National Hospital Organization Kyushu Medical Center, Fukuoka, Japan;
[4] Hitachi, Ltd. Hitachi Health Care Center, Ibaraki, Japan.

Abstract: The visceral fat area obtained by computed tomography (CT) at the navel level is clinically used as an indicator of visceral fat obesity in Japan. Analysis of skeletal muscle mass using CT images at the navel level may potentially support concurrent assessment of sarcopenia and sarcopenic obesity. The purpose of this study was to assess the performance of deep learning models (DLMs) for skeletal muscle mass measurement using low-dose abdominal CT. The primary dataset used in this study included 11,494 low-dose abdominal CT images at navel level acquired in 7,370 subjects for metabolic syndrome screening. The publicly available Cancer Imaging Archive (TCIA) dataset, including 5,801 abdominal CT images, was used as a complementary dataset. For abdominal CT image segmentation, we used the SegU-net DLM with different filter size and hierarchical depth. The segmentation accuracy was assessed by measuring the dice similarity coefficient (DSC), cross-sectional area (CSA) error, and Bland-Altman plots. The proposed DLM achieved a DSC of 0.992 ± 0.012, a CSA error of 0.41 ± 1.89%, and a Bland-Altman percent difference of -0.1 ± 3.8%. The proposed DLM was able to automatically segment skeletal muscle mass measurements from low-dose abdominal CT with high accuracy.

***Keywords*:** deep learning, low-dose CT, skeletal muscle, image segmentation, sarcopenia

Introduction

Sarcopenia is a condition introduced by Rosenberg in 1989, and it refers to a decline in mass of skeletal muscle and reduced strength of muscles in the whole body, resulting in reduced physical performance. Frequently, sarcopenia occurs naturally due to aging. The term sarcopenia is derived from the Greek words "sarx" (muscle) and "penia" (loss) (*1*).

It has become clear that sarcopenia not only threatens the healthy life expectancy of the elderly, but it is also associated with various diseases and it may affect their prognosis. For example, the survival of individuals with solid tumors is worse if the skeletal muscle mass is lower (*2*). Moreover, patients with low muscle mass have been reported to be more likely to accumulate treatment-related events (*3,4*). In addition, sarcopenic obesity, which refers to a combination of skeletal muscle mass weakening and body fat accumulation, has become a topic issue in recent years. Patients with sarcopenic obesity have a higher prevalence of dyslipidemia than those with sarcopenia alone or obesity alone (*5*). The odds ratio of hypertension is equal to 1.5 in patients with sarcopenia compared to healthy subjects, and it becomes 2.08 times higher in patients with obesity and 3.0 times higher in patients with sarcopenic obesity (*6*). The odds ratio of metabolic syndrome is 1.98 times higher in patients with sarcopenia, and it becomes 7.53 times higher in patients with obesity, and 11.59 times higher in patients with sarcopenic obesity compared to healthy subjects (*7*).

One of the diagnostic indicators for sarcopenia is skeletal muscle mass. Skeletal muscle mass is assessed based on appendicular skeletal muscle mass measured by bioelectrical impedance analysis (BIA) or by dual-energy X-ray absorptiometry (DXA) (*8,9*). However, a high amount of adipose tissue limits the accuracy of BIA and DXA methods, as such the estimates of body composition in patients with obesity may not be accurate (*10*). Recently, single slices at various reference body levels measured by computed tomography (CT) have been adopted as a proxy for total muscle tissue volume (*11,12*). In Japan, the visceral fat area (VFA) measured by CT at the navel level is used as an indicator for visceral fat obesity, a type of obesity associated with a high risk of developing lifestyle-related diseases (*13*). Therefore, combined measurement of skeletal muscle mass in the trunk and VFA can be used to assess, concurrently,

sarcopenia, visceral fat obesity, and sarcopenic obesity.

An automated rule-based approach to VFA measurement on abdominal CT has been introduced in 2006. The use of CT images is promising in this field as CT can easily distinguish body components other than fat (*e.g.*, gas, water, blood, muscles, internal organs) by defining the fat range from -30 HU to -190 HU (*14*). Moreover, the rapid progress of deep learning algorithms, for example since Alexnet in 2012 (*15*) to U-net (*16*) in 2015, has greatly contributed to substantial developments in biomedical image segmentation and, to date, automated segmentation of skeletal muscle and other body tissues can be easily performed by using deep learning algorithms (*17-26*).

However, radiation exposure is a major barrier to widespread use of CT images and it limits the applications of CT to individual transversal images or secondary analysis of routine clinical measurements (*11*). In this context, the use of low-dose CT can help reduce issues related to human exposure and thus support a wider use of CT in diagnostics. However, the use of low-dose CT for muscle mass estimation has not been fully investigated so far (*22*). The purpose of this study was to assess the performance of deep learning for automatic skeletal muscle mass estimation using low-dose abdominal CT.

Materials and Methods

This study was conducted in accordance with the Declaration of Helsinki. Informed consent was obtained from each examinee regarding the use of his or her data for research purposes. This study was approved by the institutional review boards of Hitachi, Ltd. Hospital Management Headquarters (approval number: 2010-6). This study was based on retrospective analysis of a primary and a complementary dataset. The primary dataset included 11,494 subjects (10,241 men and 1,253 women; mean age, 57.0 ± 10.1 years), who underwent a low-dose abdominal CT at the navel level for metabolic syndrome screening at the Hitachi Health Care Center, Hitachi, Ltd. One or more images were taken around the navel level for each participant (1/2/3/4/5/6/7/8/9/10 slices = 3,349/3,925/95/0/0/0/0/0/0/1 participants). CT scans were performed at a CT dose index volume (CTDIvol) lower or equal to 2.5 mGy and an imaging range lower or equal to 5 cm, thus the exposure dose was lower or equal to 0.19 mSv. The complementary dataset was publicly available and was provided by the Cancer Imaging Archive (TCIA), funded by the Cancer Imaging Program (CIP), a part of the United States National Cancer Institute (NCI), and managed by the Frederick National Laboratory for Cancer Research (FNLCR) (*27*). This TCIA dataset included 5,801 low-dose abdominal CT images, including 2,691 slices from 22 men, 2,800 slices from 29 women, and 310 slices from 2 subjects with unspecified gender. Details of CT imaging settings of the two datasets are summarized in Table 1. The main dataset used one 5 mm-thick slice per participant, while the TCIA dataset used multiple images per examination reconstructed in finer slices of 1 to 1.25 mm.

The primary dataset was divided into Training, Tuning, and Internal validation sets and the TCIA dataset was divided into Training and Tuning sets. Training and Tuning used data taken from January 2017 to September 2018, while Internal validation used data taken from October 2018 to December 2018.

The slices for measuring skeletal muscle mass in the trunk are often measured at the 3rd lumbar spine level (*11*). However, the diagnostic index for metabolic syndrome in Japan is based on the cross-sectional area of visceral fat on abdominal CT slices at the navel level (*13*). Therefore, we built separate internal validation datasets using the upper and lower levels of the iliac crest. Details of the training, tuning, and internal validation sets are shown in Table 2.

For the sake of labeling the datasets using ground truth information, the psoas major and erector spinae muscles in each navel-level CT image were identified and manually annotated by a board-certified diagnostic radiologist (TN) with over 30 years of experience.

Our Deep learning model (DLM) was based on SegU-net (*28-30*). SegU-Net is a network structure which consists of encoders and decoders, like SegNet (*31*), linking encoder and decoder feature maps like U-Net (*16*), and using arbitrary specific hierarchies and filter sizes without cropping encoder feature maps.

We used the Exponential Linear Unit (ELU) as an activation function in the encoder and decoder processing and the max unpooling in the decoder processing. The

Table 1. CT imaging settings of the datasets used in this study

Items	Primary dataset	TCIA dataset
CT scanner	FUJIFILM Healthcare Supria Grande (64 rows)	Siemens Sensation (16 rows), Sensation (64 rows), GE LightSpeed Pro (16 rows), LightSpeed (16 rows), Philips Brilliance (40 rows)
Slice thickness	5 mm	1 to 1.25 mm
Body part	Abdomen (navel level)	Abdomen (around navel level)
Tube voltage	120 kVp	120 to 140 kVp
Tube current range	20 to 225 mA	115 to 280 mA
Low-dose CT	Yes	Yes
Pixel size (mm × mm)	(0.489 × 0.489) – (0.978 × 0.978)	(0.607 × 0.607) – (0.920 × 0.920)
Use of contrast agent	No	Yes

ELU is one of the activation functions and solves the dying Rectified Linear Unit (ReLU) problem, which showed that ReLU neurons become inactive and output only 0 for any input. The ELU contains the exponential function with the Euler number as the base, and returns a value of 0 or less if the input value is 0 or less while avoiding the ReLU-like vanishing gradient problem. The max unpooling means that the pixel value generated in the decoding process is applied to the pixel position showing the maximum value in the Max-Pooling layer in the encoding process, and all others are filled with zero. The architecture of the DLM used in this study is shown in Figure 1.

Table 2. Details of the training, tuning, and internal validation sets

Items	Training	Tuning	Internal validation	
			Upper level of iliac crest	Lower level of iliac crest
Primary dataset				
Men	7,001	1,762	1,156	322
Women	860	204	151	38
total	7,861	1,966	1,307	360
TCIA dataset				
Men	2,094	597	-	-
Women	2,180	620	-	-
Unknown	249	61	-	-
total	4,523	1,278	-	-

Original CT images were converted to normalized data of 512 × 512 size. No upper limit on the number of epochs was set. The best accuracy generation was identified at 863 epochs before overfitting was detected. Finally, 5 class regions (0: other, 1: right psoas, 2: left psoas, 3: left erector spinae, 4: right erector spinae) were defined as am image of 512 × 512 binary format.

The Dice similarity coefficient (DSC), the cross-sectional area (CSA) error and the Bland-Altman plot were performed to evaluate the segmentation performance of the proposed DLM using total and individual internal validation datasets from the upper and lower levels of the iliac crest.

The DSC was used to measure the similarity in the abdominal skeletal muscle area between the ground truth and the DLM outputs. The DSC is an index of spatial overlap ranging from 0 to 1. The DSC for the

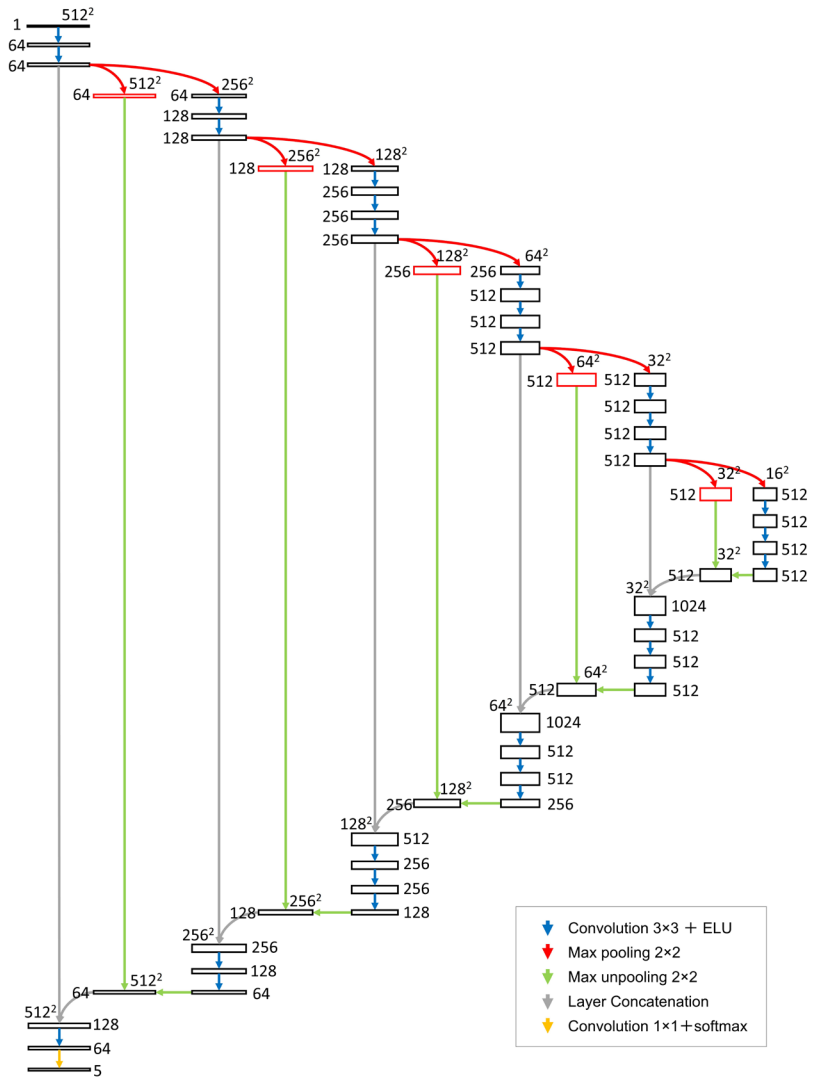

Figure 1. SegU-net architecture. Each black frame box corresponds to a multi-channel feature map. The number of channels is denoted on top or bottom of the box. The x-y-size is provided at the lower left or upper left edge of the box. Red frame boxes represent the pooling indices for max unpooling operation. The arrows denote the different operations.

combination of the right and left psoas major muscles (RPM and LPM) and for the right and left erector spinae muscles (REM and LEM) was calculated as follows.

DSC = (2 × (ground truth RPM∩calculated RPM)/ (ground truth RPM + calculated RPM) + 2 × (ground truth LPM∩calculated LPM)/ (ground truth LPM + calculated LPM) + 2 × (ground truth REM∩calculated REM)/ (ground truth REM + calculated REM)+ 2 × (ground truth LEM∩calculated LEM)/ (ground truth LEM + calculated LEM)) /4

The CSA error was also used to evaluate the segmentation accuracy of the proposed DLM. The lower the CSA error, the higher the segmentation accuracy. The CSA error for the combined muscle area (CMA) of the bilateral psoas major and erector spinae muscles calculated by the proposed DLM was computed as follows:

CSA error (%) = |ground truth CMA - calculated CMA|/ ground truth CMA ×100 (%)

The Bland-Altman plot was used to evaluate agreement between the estimated CMA and the ground truth. The mean and standard deviation (SD) of the difference between the estimated CMA and the ground truth were compared between men and women by *t*-test and F-test, respectively.

Results

The DSC was 0.992 ± 0.012, 0.993 ± 0.009, and 0.991 ± 0.019 for the total and the individual internal validation datasets from the upper and lower levels of the iliac crest, respectively. The CSA errors (%) were 0.41 ± 1.89, 0.35 ± 0.96, and 0.62 ± 3.62, respectively. The Bland-Altman plots for the CSA agreement between ground truth and DLM showed percent differences (mean ± 1.96 × SD) of -0.1 ± 3.8%, -0.05 ± 2.0%, and -0.2 ± 7.2%, respectively (Figure 2). Although there were statistically significant differences in means and SDs of the percent differences between men and women for the total (p = 0.006 and 0.008, respectively) and the upper levels of iliac crest (p = 0.0001 and < 0.0001, respectively) because of the

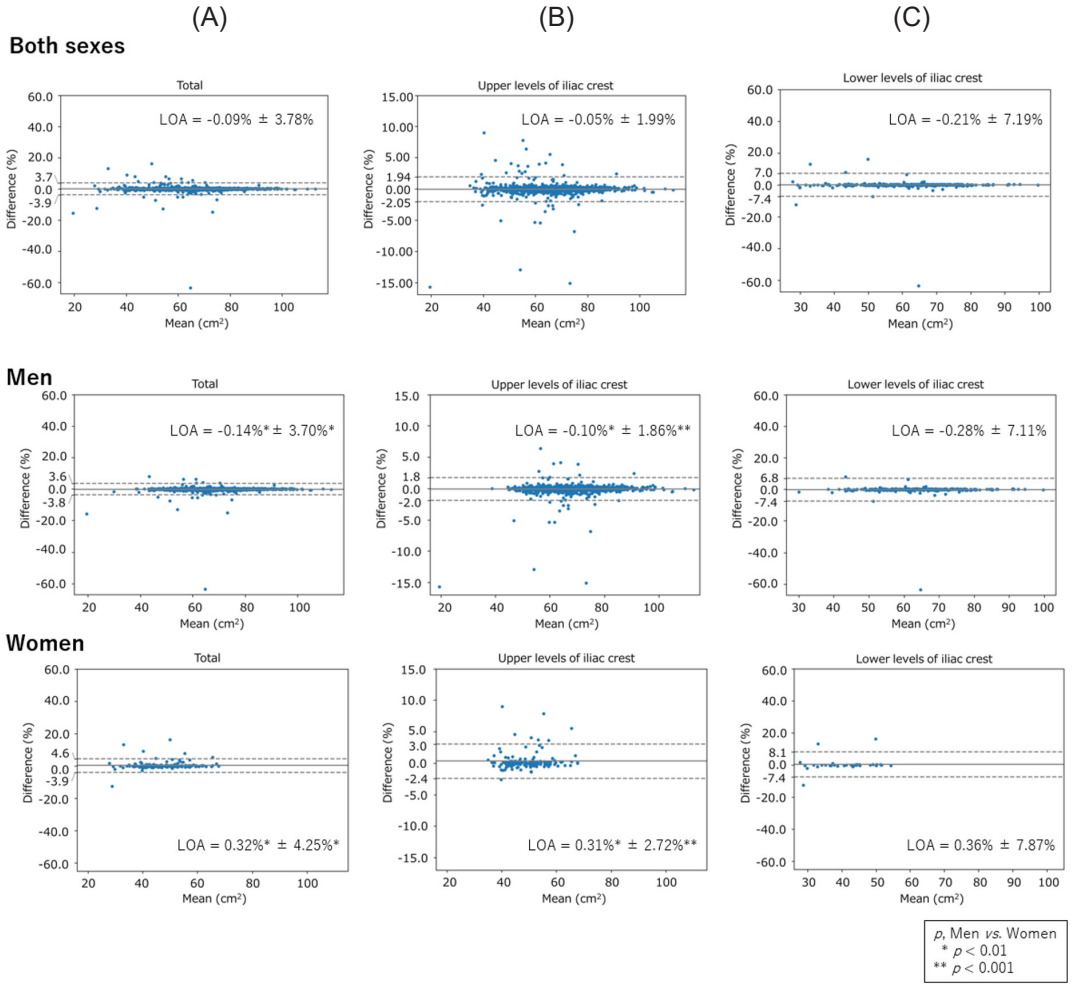

Figure 2. Bland-Altman plots for the CSA agreement between ground truth and DLM. **(A)** Total internal validation datasets, **(B)** Internal validation datasets from the upper levels of the iliac crest, **(C)** Internal validation datasets from the lower levels of the iliac crest. The solid line shows mean difference; the dotted line shows 95% limits of agreement (LOA: mean difference ± 1.96 × SD of the difference).

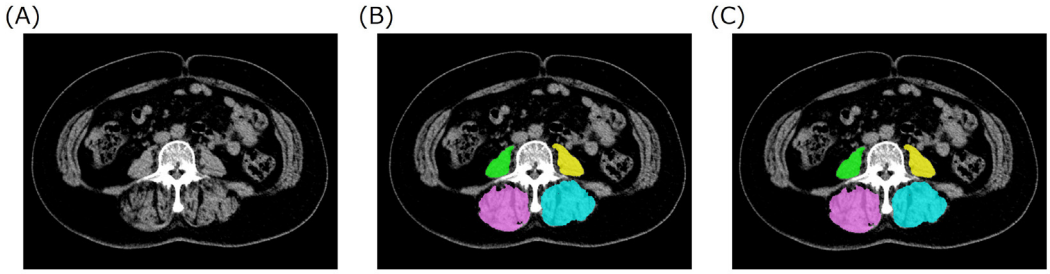

Figure 3. Example of good agreement between ground truth and DLM as DSC. (A) An original low-dose abdominal CT at navel level, **(B)** Ground truth segmentation, **(C)** DLM-derived segmentation of the right psoas major (RPM), the left psoas major (LPM), the right erector spinae (REM), and the left erector spinae (LEM) muscles in a woman's case (60 years old). Green = RPM, Yellow = LPM, Pink = REM, Blue = LEM.

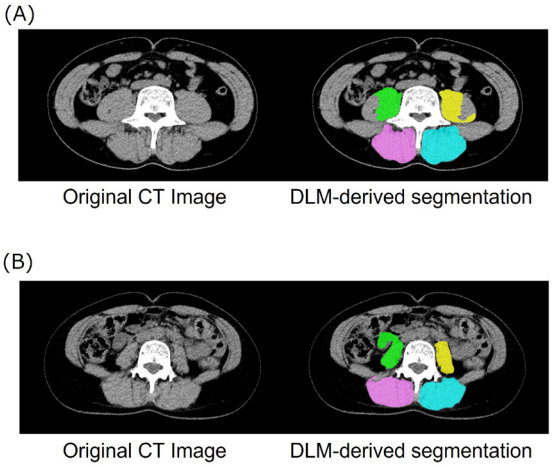

Figure 4. Cases with segmentation errors derived by the proposed DLM using internal validation dataset for the upper level of the iliac crest. (A) Case in which part of the muscle was missing, **(B)** Case in which part of the small intestine was segmented as muscle. Green = RPM, Yellow = LPM, Pink = REM, Blue = LEM.

large sample size, the differences in the actual values were very small. Figure 3 shows an exemplary case of successful segmentation of RPM, LPM, REM, and LEM.

Figure 4 shows cases with segmentation errors derived by the proposed DLM using internal validation dataset for the upper level of the iliac crest, where part of the muscle was missing or part of the small intestine was segmented as muscle.

Discussion

According to the 2019 Consensus of the Asian Working Group for Sarcopenia, the skeletal muscle mass index of the extremities using BIA and DXA is used for the diagnosis of sarcopenia in Asia (*32*). However, these measurements are not able to accurately estimate skeletal muscle mass in the trunk due to inherent limitations related to the measurement principles (*8,9*). Abdominal CT, as proposed in this study, enables measurement of the skeletal muscles of the trunk, and they can potentially become an essential technique for improving the accuracy of sarcopenia diagnosis.

However, risks related to radiation exposure represent a barrier to widespread use of CT and this imaging modality is not included in clinical recommendations for sarcopenia diagnosis. In this study, we introduced a DLM to assess skeletal muscles from low-dose CT images. The International Commission on Radiological Protection (ICRP) estimates that in a group of individuals including both adults and children, the probability of death due to cancer increases by an amount of about 0.5% per 100 mSv exposure (*33*), *i.e.* about 526 times the exposure of 0.19mSv associated with the abdominal CT scan used in this study. Future validation is needed to clarify whether the benefits of the use of low-dose CT for screening for sarcopenia and sarcopenic obesity outweigh the risks associated with radiation exposure.

Literature studies show that skeletal muscle assessment using CT scans at the level of the third lumbar (L3) spine is highly correlated with whole body skeletal muscle (*34,35*). However, this method requires adjustments on a case-by-case basis according to the target population. For example, Vangelov *et al.* (*36*) suggested to use the level of the 3rd cervical spine as an alternative because a malignant tumor confined to the head and neck usually does not require an abdominal CT. In this study, we found that the use of CT at the navel level, typically used for visceral fat area estimation in Japan, can provide accurate measurements.

The SegU-Net algorithm used here is a combination of SegNet (*31*) andU-Net (*16*). In SegNet, since encoder and decoder are connected in series, image details are lost in the process of propagating features, and the quality of segmentation of the original image is relatively low. In U-Net, the central portion of the feature map generated in each layer of the encoder is cropped to fit the feature map of the corresponding layer of the decoder. In the proposed SegU-net, the decoder uses unpooling to compensate for data deficiencies in the U-Net in place of upconvolution and cropping operations of the U-Net, to match coupling between encoder and decoder functions. In addition, in this study we also adopted the ELU as the activation function from the commonly used ReLu to solve the dying ReLU problem.

This study has several limitations. As a result of DLM-derived segmentation and validation on internal dataset by Ha *et al.* (*19*), the DSC was equal to 0.98, the CSA error (%) was equal to 1.22 ± 1.08%, and the percent difference of the Bland-Altman plots was equal to 0.2 ± 3.2%. For our DLM-derived segmentation, although DSC and CSA errors were comparable, the standard deviation observed using the total validation datasets and the validation datasets for the lower levels of the iliac crest was equal to 3.8% and 7.2%, respectively. Further research is needed to assess the variability of the observed results and to assess the distribution of the model performance, also including specific investigation of the outliers.

Moreover, the proposed DLM was not validated on external validation datasets. It will be important to identify further sources of data from different institutions to support external validation on varying datasets and assess generalization properties.

Also, in this study we did not measure the quadratus lumborum, latissimus dorsi, external oblique, internal oblique, transversus abdominis, and rectus abdominis muscles. Further studies will be necessary to assess accuracy for these muscles.

Last, but not least, the accuracy of visceral fat and subcutaneous fat measurements was not assessed. Moving towards future methods able to accurately measure sarcopenia, obesity, and sarcopenic obesity, further research is required, including specific investigation of the accuracy of visceral fat and subcutaneous fat measurements.

Conclusions

The proposed DLM was able to automatically segment skeletal muscles and assess muscle mass with high accuracy using low-dose abdominal CT images. Future research will be needed to assess the performance of the proposed method in a range of measurement settings and patient populations. The proposed DLM, may help build future automated methods to simultaneously evaluate sarcopenia, obesity, and sarcopenic obesity by measuring the navel-level visceral fat area and skeletal muscle mass using a single-slice low-dose CT.

Funding: This work was supported in part by Grants-in Aid for Research from the National Center for Global Health and Medicine (20A3002, 23A3001).

Conflict of Interest: The authors have no conflicts of interest to disclose.

References

1. Rosenberg IH. Summary comments (Epidemiologic and methodologic problems in determining nutritional status of older persons). Am J Clin Nutr. 1989; 50:1231-1233.
2. Shachar SS, Williams GR, Muss HB, Nishijima TF. Prognostic value of sarcopenia in adults with solid tumours: A meta-analysis and systematic review. Eur J Cancer. 2016; 57:58-67.
3. Antoun S, Baracos VE, Birdsell L, Escudier B, Sawyer MB. Low body mass index and sarcopenia associated with dose-limiting toxicity of sorafenib in patients with renal cell carcinoma. Ann Oncol. 2010; 21:1594-1598.
4. Raynard B, Pigneur F, Di Palma M, Deluche E, Goldwasser F. The prevalence of CT-defined low skeletal muscle mass in patients with metastatic cancer: a cross-sectional multicenter French study (the SCAN study). Support Care Cancer. 2022; 30:3119-3129.
5. Baek SJ, Nam GE, Han KD, Choi SW, Jung SW, Bok AR, Kim YH, Lee KS, Han BD, Kim DH . Sarcopenia and sarcopenic obesity and their association with dyslipidemia in Korean elderly men: The 2008-2010 Korea National Health and Nutrition Examination Survey. J Endocrinol Invest. 2014; 37:247-260.
6. Han K, Park YM, Kwon HS, Ko SH, Lee SH, Yim HW, Lee WC, Park YG, Kim MK, Park YM. Sarcopenia as a determinant of blood pressure in older Koreans: findings from the Korea National Health and Nutrition Examination Surveys (KNHANES) 2008-2010. PLoS One. 2014; 9:e86902.
7. Lu CW, Yang KC, Chang HH, Lee LT, Chen CY, Huang KC. Sarcopenic obesity is closely associated with metabolic syndrome. Obes Res Clin Pract. 2013; 7:e301-e307.
8. Sanada K, Miyachi M, Tanimoto M, Yamamoto K, Murakami H, Okumura S, Gando Y, Suzuki K, Tabata I, Higuchi M. A cross-sectional study of sarcopenia in Japanese men and women: Reference values and association with cardiovascular risk factors. Eur J Appl Physiol. 2010; 110:57-65.
9. Tanimoto Y, Watanabe M, Sun W, Hirota C, Sugiura Y, Kono R, Saito M, Kono K. Association between muscle mass and disability in performing instrumental activities of daily living (IADL) in community-dwelling elderly in Japan. Archives of gerontology and geriatrics. 2012; 54:e230-e233.
10. Jensen B, Braun W, Geisler C, Both M, Klückmann K, Müller MJ, Westphal AB. Limitations of fat-free mass for the assessment of muscle mass in obesity. Obes Facts. 2019; 12:307-315.
11. Walowski CO, Braun W, Maisch MJ, Jensen B, Peine S, Norman K, Müller MJ, Westphal AB. Reference values for skeletal muscle mass - Current concepts and methodological considerations. Nutrients. 2020; 12:755.
12. Derstine BA, Holcombe SA, Ross BE, Wang NC, Su GL, Wang SC. Skeletal muscle cutoff values for sarcopenia diagnosis using T10 to L5 measurements in a healthy US population. Sci Rep. 2018; 8:11369.
13. Examination Committee of Criteria for 'Obesity Disease' in Japan; Japan Society for the Study of Obesity. New criteria for 'obesity disease' in Japan. Circ J. 2002; 66:987-992.
14. Zhao B, Colville J, Kalaigian J, Curran S, Jiang L, Kijewski P, Schwartz LH. Automated quantification of body fat distribution on volumetric computed tomography. J Comput Assist Tomogr. 2006; 30:777-783.
15. Krizhevsky A, Sutskever I, Hinton GE. ImageNet classification with deep convolutional neural networks. *https://proceedings.neurips.cc/paper_files/paper/2012/file/c399862d3b9d6b76c8436e924a68c45b-Paper.pdf*

(accessed September 1, 2023)
16. Ronneberger O, Fischer P, Brox T. U-net: Convolutional networks for biomedical image segmentation. *https://link.springer.com/chapter/10.1007/978-3-319-24574-4_28* (accessed September 1, 2023)
17. Amarasinghe KC, Lopes J, Beraldo J, Kiss N, Bucknell N, Everitt S, Jackson P, Litchfield C, Denehy L, Blyth BJ, Siva S, MacManus M, Ball D, Li J, Hardcastle N. A deep learning model to automate skeletal muscle area measurement on computed tomography images. Front Oncol. 2021; 11:580806.
18. Cespedes Feliciano EM, Popuri K, Cobzas D, Baracos VE, Beg MF, Khan AD, Ma C, Chow V, Prado CM, Xiao J, Liu V, Chen WY, Meyerhardt J, Albers KB, Caan BJ. Evaluation of automated computed tomography segmentation to assess body composition and mortality associations in cancer patients. J Cachexia Sarcopenia Muscle. 2020; 11:1258-1269.
19. Ha J, Park T, Kim HK, Shin Y, Ko Y, Kim DW, Sung YS, Lee J, Ham SJ, Khang S, Jeong H, Koo K, Lee J, Kim KW. Development of a fully automatic deep learning system for L3 selection and body composition assessment on computed tomography. Sci Rep. 2021; 11:21656.
20. Park HJ, Shin Y, Park J, Kim H, Lee IS, Seo DW, Huh J, Lee TY, Park TY, Lee J, Kim KW. Development and validation of a deep learning system for segmentation of abdominal muscle and fat on computed tomography. Korean J Radiol. 2020; 21:88-100.
21. Perez AA, Pickhardt PJ, Elton DC, Sandfort V, Summers RM. Fully automated CT imaging biomarkers of bone, muscle, and fat: Correcting for the effect of intravenous contrast. Abdom Radiol (NY). 2021; 46:1229-1235.
22. Pickhardt PJ, Perez AA, Garrett JW, Graffy PM, Zea R, Summers RM. Fully automated deep learning tool for sarcopenia assessment on CT: L1 versus L3 vertebral level muscle measurements for opportunistic prediction of adverse clinical outcomes. AJR Am J Roentgenol. 2022; 218:124-131.
23. Weston AD, Korfiatis P, Kline TL, Philbrick KA, Kostandy P, Sakinis T, Sugimoto M, Takahashi N, Erickson BJ. Automated abdominal segmentation of CT scans for body composition analysis using deep learning. Radiology. 2019; 290:669-679.
24. Bridge CP, Rosenthal M, Wright B, *et al.* Fully-Automated Analysis of Body Composition from CT in Cancer Patients Using Convolutional Neural Networks. *https://link.springer.com/chapter/10.1007/978-3-030-01201-4_22#citeas* (accessed September 1, 2023)
25. Graffy PM, Liu J, Pickhardt PJ, Burns JE, Yao J, Summers RM. Deep learning-based muscle segmentation and quantification at abdominal CT: Application to a longitudinal adult screening cohort for sarcopenia assessment. Br J Radiol. 2019; 92:20190327.
26. Burns JE, Yao J, Chalhoub D, Chen JJ, Summers RM. A machine learning algorithm to estimate sarcopenia on abdominal CT. Acad Radiol. 2020; 27:311-320.
27. Clark K, Vendt B, Smith K, Freymann J, Kirby J, Koppel P, Moore S, Phillips S, Maffitt D, Pringle M, Tarbox L, Prior F. The Cancer Imaging Archive (TCIA): Maintaining and operating a public information repository. J Digit Imaging. 2013; 26:1045-1057.
28. Rocha J, Cunha A, Mendonça AM. Conventional filtering versus U-Net based models for pulmonary nodule segmentation in CT images. J Med Syst. 2020; 44:81.
29. Bianco M, Giri SK, Iliev IT, Mellema G. Deep learning approach for identification of H II regions during reionization in 21-cm observations. Monthly Notices of the Royal Astronomical Society. 2021; 505:3982-3997.
30. Jeon S, Choi W, Park B, Kim C. A deep learning-based model that reduces speed of sound aberrations for improved *in vivo* photoacoustic imaging. IEEE Trans Image Process. 2021; 30:8773-8784.
31. Badrinarayanan V, Kendall A, Cipolla R. Segnet: A deep convolutional encoder-decoder architecture for image segmentation. IEEE Trans Pattern Anal Mach Intell. 2017; 39:2481-2495.
32. Chen LK, Woo J, Assantachai P, *et al.* Asian Working Group for Sarcopenia: 2019 consensus update on sarcopenia diagnosis and treatment. J Am Med Dir Assoc. 2020; 21:300-307.e2.
33. Ministry of the Environment Government of Japan. BOOKLET to Provide Basic Information Regarding Health Effects of Radiation 2nd edition: Chapter 3 Health Effects of Radiation: Risks of Health Effects of Radiation. *https://www.env.go.jp/en/chemi/rhm/basic-info/1st/03.html* (accessed September 1, 2023)
34. Shen W, Punyanitya M, Wang Z, Gallagher D, St-Onge MP, Albu J, Heymsfield SB, Heshka S. Total body skeletal muscle and adipose tissue volumes: Estimation from a single abdominal cross-sectional image. J Appl Physiol (1985). 2004; 97:2333-2338.
35. Mourtzakis M, Prado CM, Lieffers JR, Reiman T, McCargar LJ, Baracos VE. A practical and precise approach to quantification of body composition in cancer patients using computed tomography images acquired during routine care. Appl Physiol Nutr Metab. 2008; 33:997-1006.
36. Vangelov B, Bauer J, Moses D, Smee R. A prediction model for skeletal muscle evaluation and computed tomography-defined sarcopenia diagnosis in a predominantly overweight cohort of patients with head and neck cancer. Eur Arch Otorhinolaryngol. 2023; 280:321-328.

Received April 12, 2023; Revised September 8, 2023; Accepted September 22, 2023.

Released online in J-STAGE as advance publication September 29, 2023.

**Address correspondence to*:
Yumi Matsushita, Department of Clinical Research, National Center for Global Health and Medicine, 1-21-1 Toyama, Shinjuku-ku, Tokyo 162-8655, Japan.
E-mail: ymatsushita@hosp.ncgm.go.jp